Tm 3+ -doped calcium lithium tantalum gallium garnet (Tm:CLTGG): novel laser crystal

Adrian Alles, Zhongben Pan, Pavel Loiko, Josep Maria Serres, Sami Slimi, Shawuti Yingming, Kaiyang Tang, Yicheng Wang, Yongguang Zhao, Elena Dunina, et al.

Tm^{3+}-doped calcium lithium tantalum gallium garnet (Tm:CLTGG): Novel laser crystal

ADRIAN ALLES,[1,2] ZHONGBEN PAN,[3,4] PAVEL LOIKO,[5] JOSEP MARIA SERRES,[1,2] SAMI SLIMI,[1] SHAWUTI YINGMING,[3] KAIYANG TANG,[3] YICHENG WANG,[4] YONGGUANG ZHAO,[4,6] ELENA DUNINA,[7] ALEXEY KORNIENKO,[7] PATRICE CAMY,[5] WEIDONG CHEN,[4,8] LI WANG,[4] UWE GRIEBNER,[4] VALENTIN PETROV,[4] ROSA MARIA SOLÉ,[1] MAGDALENA AGUILÓ,[1] FRANCESC DÍAZ[1] AND XAVIER MATEOS[1,#,*]

[1]*Universitat Rovira i Virgili, FiCMA-FiCNA, Marcel·lí Domingo 1, 43007 Tarragona, Spain*
[2]*Eurecat, Centre Tecnològic de Catalunya, Advanced Manufacturing Systems Unit (AMS), Marcel·lí Domingo 2, 43007 Tarragona, Spain*
[3]*Institute of Chemical Materials, China Academy of Engineering Physics, 621900 Mianyang, China*
[4]*Max Born Institute for Nonlinear Optics and Short Pulse Spectroscopy, Max-Born-Str. 2a, 12489 Berlin, Germany*
[5]*Centre de Recherche sur les Ions, les Matériaux et la Photonique (CIMAP), UMR 6252 CEA-CNRS-ENSICAEN, Université de Caen Normandie, 6 Boulevard du Maréchal Juin, 14050 Caen Cedex 4, France*
[6]*Jiangsu Key Laboratory of Advanced Laser Materials and Devices, Jiangsu Normal University, 221116 Xuzhou, China*
[7]*Vitebsk State Technological University, 72 Moskovskaya Ave., 210035 Vitebsk, Belarus*
[8]*Fujian Institute of Research on the Structure of Matter, Chinese Academy of Sciences, Fuzhou, 350002 Fujian, China*
[#]*Serra Húnter Fellow, Spain*
**Corresponding author email: xavier.mateos@urv.cat*

Abstract: We report on the development of a novel laser crystal with broadband emission properties at ~2 μm – a Tm^{3+},Li^{+}-codoped calcium tantalum gallium garnet (Tm:CLTGG). The crystal is grown by the Czochralski method. Its structure (cubic, sp. gr. $Ia\bar{3}d$, a = 12.5158(0) Å) is refined by the Rietveld method. Tm:CLTGG exhibits a relatively high thermal conductivity of 4.33 $Wm^{-1}K^{-1}$. Raman spectroscopy confirms weak concentration of vacancies due to the charge compensation provided by Li^{+} codoping. The transition probabilities of Tm^{3+} ions are determined using the modified Judd-Ofelt theory yielding the intensity parameters Ω_2 = 5.185, Ω_4 = 0.650, Ω_6 = 1.068 [10^{-20} cm^2] and α = 0.171 [10^{-4} cm]. The crystal-field splitting of the Tm^{3+} multiplets is revealed at 10 K. The first diode-pumped Tm:CLTGG laser generates 1.08 W at ~2 μm with a slope efficiency of 23.8%. The Tm^{3+} ions in CLTGG exhibit significant inhomogeneous spectral broadening due to the structure disorder (a random distribution of Ta^{5+} and Ga^{3+} cations over octahedral and tetrahedral lattice sites) leading to smooth and broad gain profiles (bandwidth: 130 nm) extending well above 2 μm and rendering Tm:CLTGG suitable for femtosecond pulse generation.

1. Introduction

An ordered crystal is an ideal solid state material exhibiting lattice periodicity in all directions. The certain arrangement of atoms in the unit-cell is repeated forming a translationally invariant crystal structure in the long-range. A disorder of the structure denotes some deviation from a perfect crystalline order. Weak disorder can be represented as a perturbation of the crystalline structure, e.g., caused by dopants, defects, vacancies and / or dislocations. Strong disorder is a

pronounced departure from the crystalline order. The length scale over which order, or disorder persists is also relevant. The local disorder can be revealed at a length of several unit-cells.

In laser physics, structurally disordered crystals constitute an important class of gain materials [1]. In such crystals, one or several host-forming cations are randomly distributed over two or more different crystallographic sites. Two situations for the dopant (laser-active) ions can be thus distinguished: (i) the dopant ions are distributed over several lattice sites [1] or (ii) they are present at one site while other cations experience a random site distribution [2]. In both cases, the spectral bands of dopant ions will experience an inhomogeneous broadening either due to the presence of several crystal-fields or due to the different cation multi-ligands around the dopant ions. Such spectral broadening is favorable for broad tuning of the laser wavelength and / or the generation of ultrashort pulses in mode-locked (ML) lasers. Note that there also exists compositional disorder in "mixed" (solid-solution) materials $A_{1-x}B_x$, even when the parent compounds (A and B) are ordered [3]. This also results in spectral broadening. The main drawback of disordered crystals is the deterioration of their thermal properties which justifies the search for such crystals with high thermal conductivity.

Among the host crystals for doping with laser-active rare-earth ions (RE^{3+}), cubic multicomponent garnets with general chemical formula $\{A\}_3[B]_2(C)_3O_{12}$ where A = Y, Gd, Lu or Ca, Mg, Fe, Sr, etc., and B and C = Al, Sc, Ga, Ta, etc., occupy a special position. Note that the ordered garnet $Y_3Al_5O_{12}$ (YAG) is the most widespread laser host crystal. Crystals belonging to the cubic garnet family combine good thermo-mechanical behavior with attractive spectroscopic properties of the dopant RE^{3+} ions. They are optically isotropic. Finally, cubic garnets can be grown by the well-developed Czochralski (Cz) method.

Among the structurally disordered multicomponent garnets, calcium niobium gallium garnet (CNGG) is one of the best known representatives [4,5]. The structure disorder of CNGG originates from a random distribution of Nb^{5+} and Ga^{3+} cations over [B] and (C) lattice sites leading to a significant inhomogeneous broadening of the emission bands of the RE^{3+} dopant ions. The latter are expected to replace for the divalent Ca^{2+} cations; the charge compensation is provided by vacancies [6] or by intentional codoping by univalent alkali ions (Na^+, Li^+ or their combination) [7,8] further affecting the spectral broadening [9].

Recently, CNGG-type crystals doped with thulium (Tm^{3+}) [10] and holmium (Ho^{3+}) [11] ions have proven to be very suitable for the generation of sub-100 fs pulses at ~2 μm owing to their smooth and very broad gain profiles extending beyond the structured water vapor air absorption [12] which is essential for the broadband ML laser performance. Pan *et al*. reported on a Tm,Na:CNGG (Tm:CNNGG) laser mode-locked by a single-walled carbon nanotube saturable absorber (SA) delivering 84-fs pulses at 2018 nm [10]. In the continuous-wave (CW) regime, a broad tuning range of 1879 – 2086 nm was achieved in the same work [10]. Zhao *et al.* achieved shorter pulses (67 fs, i.e., 10 optical cycles at 2083 nm) from a Tm,Ho,Li:CNGG (Tm,Ho:CLNGG) laser ML by the same SA utilizing the combined gain bandwidths from both active ions [13].

There exists another disordered multicomponent garnet similar to CNGG, namely calcium tantalum gallium garnet (CTGG) [14]. Ma *et al*. have shown that CTGG exhibits higher thermal conductivity (κ = 3.76 $Wm^{-1}K^{-1}$) as compared to its niobium counterpart [14]. CTGG-type crystals doped with Nd^{3+} and Yb^{3+} ions have been studied for laser operation at ~1 μm [15,16]. However, no lasing in the ~2 μm spectral range has been reported so far.

In the present work, we reveal the potential of Tm^{3+}, Li^+-codoped CTGG (abbreviated Tm:CLTGG) as a broadband laser gain material at ~2 μm and beyond.

2. Crystal growth

A Tm:CLTGG single crystal was grown by the Czochralski (Cz) method in an iridium crucible using argon atmosphere. The starting materials, $CaCO_3$ (purity: 4N), Ta_2O_5, Ga_2O_3, Li_2CO_3 and Tm_2O_3 (purity: 5N), were weighed according to the following chemical formula: $Ca_3Ta_{1.88}Li_{0.20}Ga_{2.80}O_{12}{\cdot}0.05Tm_3Ga_5O_{12}$. To compensate the volatilization of Ga_2O_3 during the

synthesis of the polycrystalline material and the crystal growth, an excess of 1.0 wt% Ga_2O_3 was used. Larger excess of Ga_2O_3 violates the composition of the crystal and affects its optical quality. The equation of the chemical reaction reads:

$$3CaCO_3 + 0.94Ta_2O_5 + 1.525Ga_2O_3 + 0.075Tm_2O_3 + 0.1Li_2CO_3 \rightarrow$$
$$Ca_3Ta_{1.88}Li_{0.20}Ga_{2.80}O_{12}\cdot 0.05Tm_3Ga_5O_{12} + 3.1CO_2\uparrow.$$

The raw materials were mixed, ground and heated at 900 °C for 10 h in a platinum crucible to decompose $CaCO_3$. After cooling down the crucible to room temperature (RT, 20 °C), the mixture was pressed into tablets and reheated at 1200 °C for 15 h to form the cubic garnet phase through a solid-state reaction. The synthesized polycrystalline material was placed in an iridium crucible and melted by an intermediate-frequency heater. The first crystal was grown using an [111] oriented seed from undoped YAG. From this first crystal, another seed with the same orientation was cut and used for the growth of laser-quality crystals. During the crystal growth, the pulling rate varied from 0.5 to 1.0 mm/h and the crystal rotation speed was kept at 8 to 15 revolutions per minute. Once the growth was completed, the crystal was removed from the melt and cooled down to RT at a stepped rate of 15 to 25 °C/h. The crystal was annealed in air, the maximum temperature was 1200 °C and the hold duration was 24 h, the heating and cooling rates were about 50 °C/h.

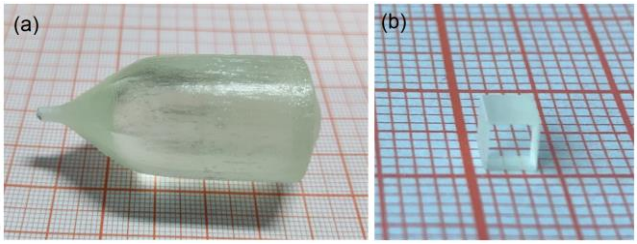

Fig. 1. (a) Photograph of the as-grown Tm:CLTGG crystal boule, the growth direction is [111]; (b) photograph of a polished laser element.

Figure 1 shows a photograph of an as-grown Tm:CLTGG crystal boule. It has a cylindrical shape (diameter: 20 mm, length of the central part: 30 mm). The crystal does not contain cracks and inclusions and no scatter centers are seen under illumination by a He-Ne laser indicating good optical quality. The as-grown crystal shows a light greenish coloration. The surface of the boule is translucent probably due to the volatilization of Ga_2O_3 during the crystal growth (it may attack the surface of the crystal that is pulled over the melt). The internal part of the crystal exhibits excellent transparency, Fig. 1(b).

By using X-ray fluorescence, the actual concentration of Tm^{3+} ions was measured to be 3.17 at.% with respect to Ca^{2+} ions ($N_{Tm} = 5.03\times10^{20}$ cm^{-3}) leading to a segregation coefficient K_{Tm} of 0.67. The targeted doping concentration of ~3 at.% Tm was selected due to the spectroscopic considerations. It could be further increased by changing the Tm content in the growth batch considering the determined K_{Tm} value.

3. Crystal structure

3.1 X-ray diffraction

The X-ray powder diffraction (XRD) pattern was measured at RT using a Bruker D2 Phaser diffractometer, Cu Kα1 radiation (1.54184 Å) with a step size of 0.02° and a step time of 1.0 s, in the range of 2θ from 10° to 90°. The measured diffraction pattern, Fig. 2(a), agrees well with the theoretical one for cubic $Al_{1.23}Ca_3Fe_{0.99}Hf_2Si_{0.99}O_{12}$ garnet (Crystallography Open Database (COD) card #96-901-3967). No other phases are found.

The structure of Tm:CLTGG was refined using the Rietveld method. The Match3! software was used and a total of 196 reflections were analyzed. The obtained reliability factors are R_p = 4.94%, R_{wp} = 6.38%, R_{exp} = 2.21% and the reduced chi squared $\chi^2 = (R_{wp}/R_{exp})^2$ = 8.37.

Tm:CLTGG crystallizes in the cubic class (sp. gr. $Ia\bar{3}d$, No. 230) with a lattice constant a = 12.5158(0) Å, the volume of the unit-cell is V = 1960.54 Å^3, the calculated density is ρ_{calc} = 5.893 g/cm^3 and the number of formula units in the unit-cell is Z = 8. The fractional atomic coordinates, the site occupancy factors (O.F.) and the isotropic displacement parameters obtained during the Rietveld refinement are listed in Table 1.

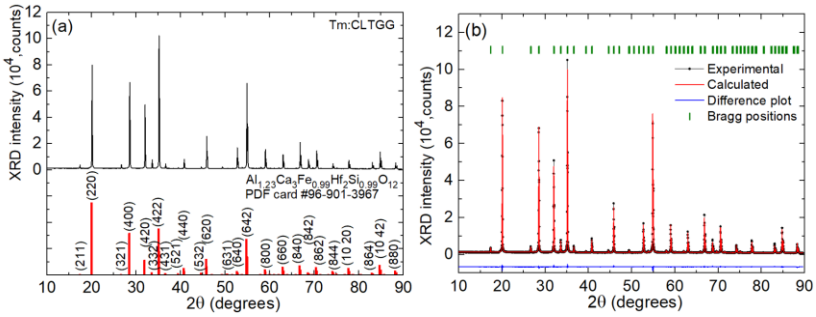

Fig. 2. X-ray powder diffraction study of Tm:CLTGG: (a) XRD pattern, (*hkl*) are Miller's indices, *vertical bars* – theoretical pattern for $Al_{1.23}Ca_3Fe_{0.99}Hf_2Si_{0.99}O_{12}$ garnet; (b) Rietveld structure refinement: experimental (*black*), calculated (*red*) and differential (*blue*) XRD profiles, *vertical dashes* mark the Bragg reflections.

Table 1. Fractional Atomic Coordinates, Occupancy Factors and Isotropic Displacement Parameters for Tm:CLTGG Crystal

Atoms	Wyckoff	*x*/*a*	*y*/*b*	*z*/*c*	O.F.	B_{iso}, Å^2
Ca	24*c*	1/8	0.0000(0)	1/4	0.963	0.722(7)
Tm	24*c*	1/8	0.0000(0)	1/4	0.031	0.722(7)
Ta1	16*a*	0.0000(0)	0.0000(0)	0.0000(0)	0.660	0.253(1)
Ga1	16*a*	0.0000(0)	0.0000(0)	0.0000(0)	0.340	0.253(1)
Ga2	24*d*	0.3750(0)	0.0000(0)	1/4	0.789	0.481(4)
Ta2	24*d*	0.3750(0)	0.0000(0)	1/4	0.068	0.481(4)
Li	24*d*	0.3750(0)	0.0000(0)	1/4	0.115	0.481(4)
O	96*h*	-0.0295(1)	0.0492(1)	0.1482(9)	1	0.826(0)

The structure of Tm:CLTGG is illustrated in Fig. 3. This crystal belongs to the family of multicomponent garnets with a general formula $\{A\}_3[B]_2(C)_3O_{12}$, where {A}, [B], and (C) stand for dodecahedral (Wyckoff symbol: 24*c*), octahedral (16*a*) and tetrahedral (24*d*) sites, respectively [5]. The stoichiometric CTGG, in analogy to CNGG [4], is expected to have a chemical formula of $Ca_3Ta_{1.5}Ga_{3.5}O_{12}$ which is equivalent to $\{Ca_3\}[Ta_{1.5}Ga_{0.5}](Ga_3)O_{12}$. The composition of the real crystal (even undoped) deviates from the stoichiometric one. The Ca^{2+} cations are located in the {A} sites.

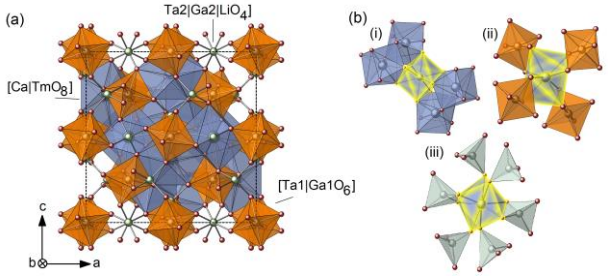

Fig. 3. Crystal structure of Tm:CLTGG: (a) a fragment of the crystal structure within one unit-cell (*dashed lines*) in projection to the ***a*-*c*** plane; (b) the variety of cationic distributions around Ca^{2+} | Tm^{3+} ions occupying the dodecahedral 24*c* sites: nearest-neighbor cations at: (i) dodecahedral 24*c* sites, (ii) octahedral 16*a* sites and (iii) tetrahedral 24*d* sites.

The Tm^{3+} ions replace for the Ca^{2+} ones (the corresponding ionic radii are R_{Ca} = 1.12 Å and R_{Tm} = 0.994 Å for VIII-fold oxygen coordination). In the [Ca|TmO_8] dodecahedrons, there are four shorter (2.3966(2) Å) and four longer (2.5577(0) Å) metal-to-oxygen (M-O) interatomic distances. The Ta^{5+} and Ga^{3+} cations are randomly distributed over the [B] and (C) sites with VI-fold and IV-fold oxygen coordination, respectively, according to the occupancy factors listed in Table 1. The M-O bond lengths are 1.990(0) Å (×6) and 1.8526(1) Å (×4), respectively. The Li^+ ion incorporation in this garnet takes place only at 24*d* sites. The charge compensation is ensured by both, Li^+ ions and cationic vacancies □ in the 24*c* and 24*d* sites. Their calculated percentages are 0.6% and 2.8%, respectively. The chemical formula of the crystal can be thus expressed as follows:

$\{Ca_{2.889}Tm_{0.093}\square_{0.018}\}[Ta_{1.32}Ga_{0.68}](Ga_{2.367}Ta_{0.204}Li_{0.345}\square_{0.084})O_{12}$.

In the Tm:CLTGG structure, each [Ca|TmO_8] dodecahedron shares edges with four other dodecahedra where the shortest interatomic distance Ca|Tm—Ca|Tm is 3.8321(1) Å, and it is surrounded by four corner-sharing octahedra (Ta^{5+} and Ga^{3+} at 16*a* sites) and by six tetrahedra (Ga^{3+}, Ta^{5+} and Li^+ at 24*d* sites), two of them sharing edges, and the remaining four being connected by shared corners.

3.2 Raman spectroscopy

The Raman spectrum of Tm:CLTGG was measured using a Renishaw inVia confocal Raman microscope with a ×50 Leica objective and an Ar^+ ion laser (514 nm). It is shown in Fig. 4. In the same figure, for comparison, we also show the Raman spectrum of its niobium isomorph, Tm:CLNGG. A total of 18 bands are resolved in the Raman spectrum of Tm:CLTGG. Among them, the vibrations at high frequencies (700-900 cm^{-1}) forming two broad bands are typically analyzed as they are sensitive to the alteration of the structure of multicomponent garnets [4,5]. They are assigned to internal vibrations (symmetric stretching modes, ν_s) of [$M2O_4$] tetrahedra (M2 = Ga2 and Ta2). In our case, the tetrahedral sites (24*d*) are occupied by Ta^{5+} and Ga^{3+} cations. The band at lower frequencies with two local maxima at 748 cm^{-1} (C_1) and 772 cm^{-1} (C_2), is assigned to the [$Ga2O_4$] groups and it is only slightly distorted with respect to that in the Tm:CLNGG crystal. The band at higher frequencies, at 842 cm^{-1} (C_4), is due to the [$Ta2O_4$] groups. The latter does not split, possesses much weaker intensity and is shifted to higher frequencies as compared to that in Tm:CLNGG crystal with [$Nb2O_4$] groups. The lack of the long-frequency component of the second band indicates weak structural distortion of the [$Ta2O_4$] tetrahedra and weak content of cationic vacancies, in agreement with the XRD study. This highlights the positive role of Li^+ ions in the charge compensation.

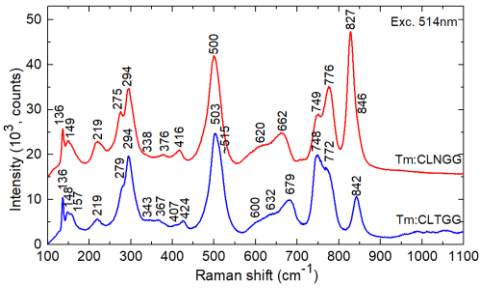

Fig. 4. Unpolarized RT Raman spectrum of the Tm:CLTGG crystal, λ_{exc} = 514 nm. *Numbers* indicate the band frequencies in cm^{-1}. The Raman spectrum of Tm:CLNGG is given for comparison.

4. Thermal properties

The specific heat C_p and the thermal diffusivity λ were measured using a laser flash apparatus (NETZSCH LFA457). For this, a squared wafer with dimensions of 4×4×1 mm^3 was cut from the Tm:CLTGG crystal along the [111] direction and double side coated with graphite.

The dependence of the specific heat (C_p) of Tm:CLTGG on temperature is shown in Fig. 5(a). The C_p value increases monotonously with temperature, from 0.57 to 0.66 J g^{-1} K^{-1}, when the temperature is increased from 298.2 K to 571.9 K. Figure 5(b) shows the measured thermal diffusivities (λ). The λ value along the [111] direction decreases with temperature. At 298.2 K, it amounts to 1.374 mm^2/s. Finally, the thermal conductivity along the [111] direction was calculated using the formula $\kappa = \lambda \times \rho \times C_p$ where ρ = 5.53 g/cm^3 is the crystal density measured using the buoyancy method. The thermal conductivity decreases with temperature, Fig. 5(c). At room temperature, it amounts to 4.33 $Wm^{-1}K^{-1}$, which is larger than for CNGG-type crystals [4,20]. The value of thermal conductivity for Tm:CLTGG is higher than that for undoped CTGG (3.76 $Wm^{-1}K^{-1}$) [14]. We refer this to the effect of Li^+ codoping on eliminating the cationic vacancies and increasing the thermal conductivity. This effect seems to overcome the negative role of rare-earth doping which typically tends to decrease κ.

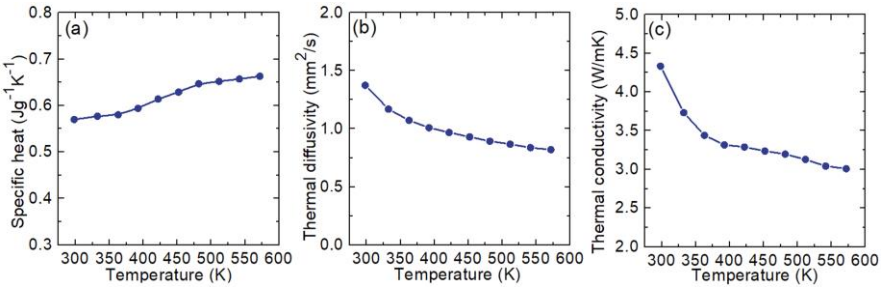

Fig. 5. Thermal properties of the Tm:CLTGG crystal as a function of temperature: (a) specific heat; (b) thermal diffusivity; (c) thermal conductivity.

5. Optical spectroscopy

5.1 Optical absorption

The absorption spectrum was measured using a Varian CARY 5000 spectrophotometer. The cubic Tm:CLTGG is optically isotropic. The unpolarized RT absorption spectrum of Tm:CLTGG is shown in Fig. 6(a). In the spectrum, the well-resolved absorption bands are related to transitions of Tm^{3+} ions from the ground-state ($^3H_6$) to excited-states (from $^3F_4$ to $^1D_2$, in increasing energy order).

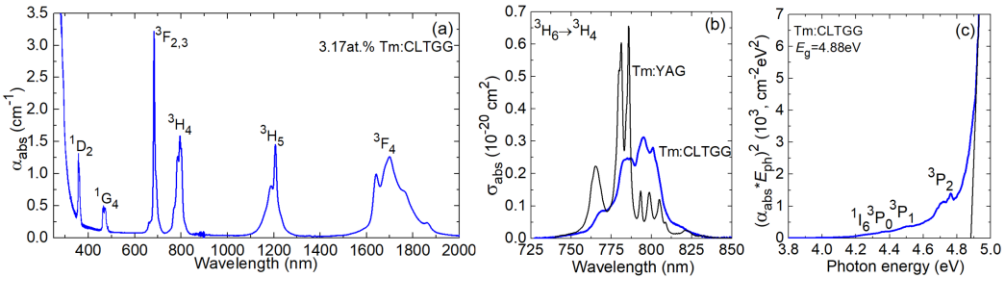

Fig. 6. Absorption of the Tm:CLTGG crystal: (a) RT absorption spectrum; (b) absorption cross-sections, σ_{abs}, for the $^3H_6 \rightarrow {}^3H_4$ Tm^{3+} transition; (c) Tauc plot for the evaluation of the optical bandgap (E_g).

The absorption cross-sections σ_{abs} for the $^3H_6 \rightarrow {}^3H_4$ Tm^{3+} transition which is suitable for pumping of laser crystals by AlGaAs diode lasers emitting at ~0.8 μm are shown in Fig. 6(b). The maximum σ_{abs} is 0.31×10^{-20} cm^2 at 795.0 nm and the absorption bandwidth (full width at half maximum, FWHM) is 26.7 nm. Compared to the widespread Tm:$Y_3Al_5O_{12}$ garnet crystal, Tm:CLTGG exhibits smoother and broader absorption at the expense of lower cross-section.

This represents the effect of inhomogeneous broadening caused by the structural disorder and, in particular, the different cationic distributions around the Tm^{3+} ions, cf. Fig. 3(b).

The absorption spectrum of Tm:CLTGG reveals no significant absorption in the visible from color centers related to cationic vacancies. This indicates charge compensation via Li^+ doping. Figure 6(c) shows the Tauc plot for the determination of the UV absorption edge (assuming indirect transitions). The optical bandgap energy E_g is 4.88 eV (0.254 μm). At the onset of the host absorption, weak absorption bands due to transitions of Tm^{3+} ions to higher-lying $^1I_6$ and $^3P_{0\text{-}2}$ states are found.

5.2 Judd-Ofelt analysis

The transition intensities for Tm^{3+} ions were calculated from the absorption spectrum using the standard Judd-Ofelt (J-O) theory [17,18], and its modification accounting for configuration interaction (mJ-O theory) [19]. This formalism was used to determine the contributions of electric dipoles (ED). The magnetic dipole (MD) contributions for transitions with $\Delta J = J - J' = 0, \pm 1$ were calculated independently within the approximation of Russell–Saunders on the wave functions of Tm^{3+} under an assumption of a free-ion. The refractive index of CLTGG was taken from [20].

The detailed procedure of the J-O calculations for Tm^{3+}-doped crystals is described in detail elsewhere [21]. Here, we only discuss the main approximations. For the standard J-O theory, the ED line strengths of the $J \rightarrow J'$ transition are given by:

$$S_{\text{calc}}^{\text{ED}}(JJ') = \sum_{k=2,4,6} U^{(k)}\Omega_k, \tag{1a}$$

$$U^{(k)} = \langle (4f^n)SLJ \,\|\, U^k \,\|\, (4f^n)S'L'J' \rangle^2 . \tag{1b}$$

Here, $U^{(k)}$ are the reduced squared matrix elements which were calculated using the free-ion parameters from [22] and Ω_k are the intensity (J–O) parameters (for both, $k = 2, 4, 6$).

In the mJ-O theory, it is assumed that only the excited configuration of opposite parity $4f^{n-1}5d^1$ contributes to the configuration interaction. The ED line strengths are then [19]:

$$S_{\text{calc}}^{\text{ED}}(JJ') = \sum_{k=2,4,6} U^{(k)}\tilde{\Omega}_k , \tag{2a}$$

$$\tilde{\Omega}_k = \Omega_k[1 + 2\alpha(E_J + E_{J'} - 2E_f^0)]. \tag{2b}$$

In other words, the intensity parameters $\tilde{\Omega}_k$ are linear functions of energies (E_J and $E_{J'}$) of the two multiplets, where E_f^0 is the mean energy of the $4f^n$ configuration and $\alpha \approx 1/(2\Delta)$ where $\Delta \approx E(4f^{n-1}5d^1) - E(4f^n)$ is the average energy difference between the fundamental and first excited configurations.

Table 2. Measured and Calculated Absorption Oscillator Strengths of Tm^{3+} ions in CLTGG crystal[a]

Transition $^3H_6 \rightarrow {}^{2S+1}L_J$	$\langle E \rangle$, cm^{-1}	Γ, $nm \times cm^{-1}$	f_{exp}, 10^{-6}	f^{Σ}_{calc}, 10^{-6} J-O	mJ-O
$^3F_4$	5823	215.51	1.641	1.649^{ED}	1.583^{ED}
$^3H_5$	8363	76.642	1.211	$1.317^{ED}+0.534^{MD}$	$1.058^{ED}+0.534^{MD}$
$^3H_4$	12628	51.696	1.859	2.139^{ED}	2.810^{ED}
$^3F_{3,2}$	14568	44.848	2.137	3.073^{ED}	2.521^{ED}
$^1G_4$	21182	7.750	0.791	0.568^{ED}	1.101^{ED}
$^1D_2$	27686	10.607	1.849	1.815^{ED}	1.783^{ED}
$^1I_6+{}^3P_0+{}^3P_1$	35239	13.677	3.811	$1.690^{ED}+0.029^{MD}$	$3.017^{ED}+0.029^{MD}$
$^3P_2$	38067	6.665	2.166	1.958^{ED}	2.270^{ED}
r.m.s. dev.				*1.078*	*0.689*

[a] $\langle E \rangle$ - "center of gravity" of the absorption band, Γ – integrated absorption coefficient, f_{exp} and f^{Σ}_{calc} – experimental and calculated absorption oscillator strengths, respectively, ED electric-dipole, MD - magnetic-dipole.

Table 2 summarizes the experimental and calculated absorption oscillator strengths *f* (the latter are determined by both the J-O and mJ-O theories from the corresponding line strengths). The intensity parameters are $\Omega_2 = 1.715$, $\Omega_4 = 0.943$ and $\Omega_6 = 0.963$ [10^{-20} cm^2] (J-O theory) and $\Omega_2 = 5.185$, $\Omega_4 = 0.650$, $\Omega_6 = 1.068$ [10^{-20} cm^2] and $\alpha = 0.171$ [10^{-4} cm] (mJ-O theory). The latter theory provides lower root mean square (rms) deviation between the experimental and calculated *f* values, so that it was selected for further analysis.

The probabilities of spontaneous radiative transitions A_{calc}(JJ'), the luminescence branching ratios B(JJ') and the radiative lifetimes of the excited-states τ_{rad} were calculated using the mJ-O theory, the results are shown in Table 3. For the $^3F_4$ and $^3H_4$ states, τ_{rad} is 5.33 ms and 0.55 ms, respectively.

Table 3. Calculated Probabilities of Spontaneous Radiative Transitions of Tm^{3+} ions in CLTGG crystal (Obtained from the mJ-O Theory)[a]

Excited state	Terminal state	$\langle\lambda_{em}\rangle$, nm	A_{calc}(JJ'), %	B(JJ'), %	A_{tot}, s^{-1}	τ_{rad}, ms
$^3F_4$	$^3H_6$	1717.3	63.62^{ED}	1	187.51	5.33
$^3H_5$	$^3F_4$	3937.0	$8.81^{ED}+0.24^{MD}$	0.027	329.09	3.03
	$^3H_6$	1195.7	$212.78^{ED}+107.26^{MD}$	0.973		
$^3H_4$	$^3H_5$	2344.7	$16.59^{ED}+10.34^{MD}$	0.015	1801.71	0.55
	$^4F_4$	1469.5	$154.95^{ED}+25.61^{MD}$	0.100		
	$^3H_6$	791.9	1594.22^{ED}	0.885		
$^3F_2+^3F_3$	$^3H_4$	5154.6	$22.24^{ED}+0.32^{MD}$	0.005	4760.78	0.36
	$^3H_5$	1611.6	818.37^{ED}	0.172		
	$^3F_4$	1143.5	$1191.94^{ED}+74.14^{MD}$	0.266		
	$^3H_6$	686.4	2653.77^{ED}	0.557		
$^1G_4$	$^3F_2+^3F_3$	1511.9	28.52^{ED}	0.030	4524.78	0.22
	$^3H_4$	1169.0	$103.11^{ED}+4.17^{MD}$	0.142		
	$^3H_5$	780.1	$600.49^{ED}+39.18^{MD}$	0.359		
	$^3F_4$	651.1	$1468.80^{ED}+156.71^{MD}$	0.063		
	$^3H_6$	472.1	$273.22^{ED}+12.88^{MD}$	0.406		
$^1D_2$	$^1G_4$	1537.5	563.86^{ED}	0.008	72495.29	0.01
	$^3F_2+^3F_3$	762.3	$5710.24^{ED}+183.16^{MD}$	0.081		
	$^3H_4$	664.1	5340.29^{ED}	0.074		
	$^3H_5$	517.5	218.16^{ED}	0.003		
	$^3F_4$	457.4	50840.29^{ED}	0.701		
	$^3H_6$	361.2	9639.29^{ED}	0.133		

[a] $\langle\lambda_{em}\rangle$ - mean emission wavelength, A_{calc}(JJ') – probability of radiative spontaneous transition, B(JJ') – luminescence branching ratio, A_{tot} – total probability of radiative transitions, τ_{rad} - radiative lifetime, ED electric-dipole, MD - magnetic-dipole.

5.3 Luminescence (emission spectra and lifetime)

The RT luminescence spectrum was measured using an optical spectrum analyzer (AQ6375B, Yokogawa) for which the spectral response was calibrated using a 20 W quartz iodine lamp. The pump source was a 795 nm Ti:Sapphire laser (excitation to the $^3H_4$ state). The luminescence spectrum is shown in Fig. 7(a). The broad and intense band at 1.6 - 2.3 μm is due to the $^3F_4 \rightarrow {}^3H_6$ transition, while the weaker band at 1.35 - 1.55 μm originates from the $^3H_4 \rightarrow {}^3F_4$ transition.

The luminescence decay was studied at RT using an optical parametric oscillator (Horizon, Continuum), a 1/4 m monochomator (Oriel 77200), an InGaAs detector and an 8 GHz digital oscilloscope (DSA70804B, Tektronix). The sample was finely powdered to avoid the effect of radiation trapping. The decay curve from the $^3F_4$ state is well fitted using a single-exponential law yielding a luminescence lifetime τ_{lum} of 4.93 ms (for the powdered sample), Fig. 7(b). It is only slightly shorter than the radiative one, revealing a relatively high quantum yield $\eta_q = \tau_{lum}/\tau_{rad} = 92\%$. For the bulk sample, $\tau_{lum} = 6.50$ ms due to the strong reabsorption. The decay from the $^3H_4$ state is not single-exponential revealing the effect of cross-relaxation for neighboring Tm^{3+} ions. The mean decay time $<\tau_{lum}> = 0.159$ ms, Fig. 7(c).

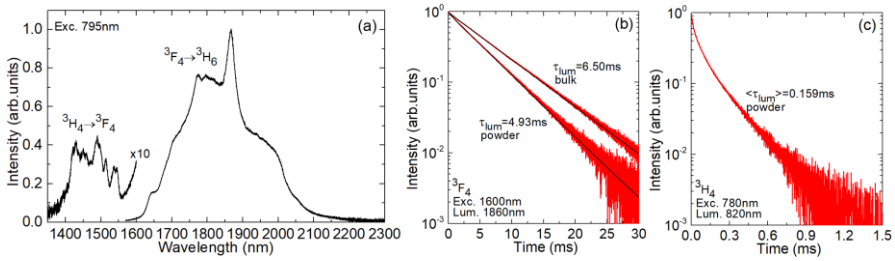

Fig. 7. Near-infrared emission properties of the Tm:CLTGG crystal: (a) luminescence spectrum, λ_{exc} = 795 nm; (b,c) luminescence decay curves from the (b) $^3F_4$ and (c) $^3H_4$ Tm^{3+} states.

5.4 Low-temperature spectroscopy

The low temperature (LT, 10 K) absorption and luminescence spectra were measured using a cryostat (Oxford Instruments, model SU 12) with helium-gas close-cycle flow. In CLTGG, Tm^{3+} ions replace for the Ca^{2+} ones in dodecahedral sites with D_2 symmetry. These sites are distorted due to the presence of univalent Li^+ cations serving for charge compensation and various cation coordinations around the {A} sites, cf. Fig. 3. Each $^{2S+1}L_J$ multiplet with integer J is thus split into $2J + 1$ Stark sub-levels. For brevity, in Fig. 8, we only show the absorption and luminescence spectra revealing the splitting of the $^3F_4$ and $^3H_6$ states relevant for ~2 μm laser operation. The assignment of electronic transitions is after the work of Lupei *et al.* for ordered Tm^{3+}-doped $Gd_3Ga_5O_{12}$ (GGG) garnet [23]. Figure 8 reveals a significant inhomogeneous broadening of the absorption and luminescence bands of Tm^{3+} ions even at 10 K when the electron-phonon interaction is suppressed, which is a fingerprint of the structure disorder.

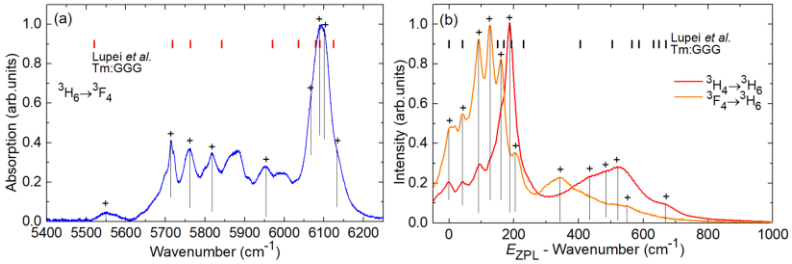

Fig. 8. Low-temperature (LT, 10 K) absorption and emission spectra for Tm^{3+} ions in the CLTGG crystal: (a) absorption, $^3H_6 \rightarrow {}^3F_4$ transition; (b) emission, $^3F_4 \rightarrow {}^3H_6$ and $^3H_4 \rightarrow {}^3H_6$ transitions. The symbol "+" marks the assigned electronic transitions. Vertical dashes – crystal-field splitting in Tm:GGG after [23].

Table 4. Experimental Energy Levels of Tm^{3+} ions in CLTGG crystal

Multiplet	E, cm^{-1}
$^3H_6$	0; 42; 91; 126; 160; 187; 206; 342; 433; 484; 522; 549; 668
$^3F_4$	5538; 5713; 5760; 5813; 5952; 6067; 6091; 6101; 6138
$^3H_5$	8299; 8314; 8396; 8412; 8426; 8458; 8567; 8606; 8683; 8773; 8809
$^3H_4$	12577; 12594; 12632; 12703; 12739; 12774; 12916; 12994; 13026
$^3F_3$	14552; 14573; 14621; 14644 (*3 missing*)
$^3F_2$	15096; 15129; 15149; 15230 (*1 missing*)
$^1G_4$	21071; 21116; 21205; 21284; 21304; 21461; 21489; 21648; 21707
$^1D_2$	27662; 27826; 27940; 28044; 28102

The experimental energy-levels of Tm^{3+} ions in CLTGG are listed in Table 4 for the multiplets from $^3H_6$ to $^1D_2$. For the $^3F_4 \rightarrow {}^3H_6$ transition of interest for ~2 μm laser operation, the zero-phonon line (ZPL), i.e., the transition between the lowest Stark sub-levels of both

multiplets, occurs at 1806 nm (E_{ZPL} = 5538 cm^{-1}). The partition functions for the ground-state and the excited-state, calculated at RT, amount to Z_1 = 4.786 and Z_2 = 2.402, respectively, so that their ratio Z_1/Z_2 = 1.992.

5.5 Transition cross-sections

The absorption cross-section spectrum for the $^3H_6 \rightarrow {}^3F_4$ transition is shown in Fig. 9(a), the maximum σ_{abs} reaches 0.25×10^{-20} cm^2 at 1699 nm.

For the $^3F_4 \rightarrow {}^3H_6$ transition, the stimulated-emission (SE) cross-section, σ_{SE}, spectra were calculated by two methods: the Füchtbauer–Ladenburg (F-L) equation [24] and the reciprocity method (RM) [25]. For the F-L equation, the luminescence spectrum was used, cf. Fig. 7(a), the radiative lifetime of the $^3F_4$ state was determined from the mJ-O theory (τ_{rad} = 5.33 ms) and the refractive index of the crystal ($n \approx 1.92$) was taken from [20]. For the RM, we used the measured absorption spectrum and the determined crystal-field splitting, cf. Table 4. The results of both methods are shown in Fig. 9(a). They are in good agreement with each other. The maximum σ_{SE} reaches 0.35×10^{-20} cm^2 at 1866 nm and at longer wavelengths where laser operation is expected, σ_{SE} reaches 0.18×10^{-20} cm^2 at 1992 nm (both values correspond to the F-L method).

The ~2 μm Tm laser represents a quasi-three-level scheme with reabsorption. Thus, gain cross-sections are usually calculated, $\sigma_{gain} = \sigma_{SE} - (1 - \beta)\sigma_{abs}$, where $\beta = N_2(^3F_4)/N_{Tm}$ is the inversion ratio. They are useful to conclude about the possible laser wavelength (in the free-running regime), the potential tuning range as well as the gain bandwidth in ML lasers. The gain spectra for Tm:CLTGG are shown in Fig. 9(b). The gain profiles of this disordered crystal are smooth and broad. For small and moderate inversion ratios ($\beta < 0.16$), a single local peak is observed in the spectra centered at ~1.99 μm. The gain bandwidth (FWHM) for an intermediate β = 0.12 is as broad as 130 nm. The gain profiles extend well beyond 2 μm owing to the large total ground-state splitting ($\Delta E(^3H_6)$ = 668 cm^{-1}) for Tm^{3+} ions and strong electron-phonon (vibronic) interaction with phonons of the host matrix. The longest purely electronic transition (neglecting the inhomogeneous broadening) for Tm^{3+} ions is 2053 nm.

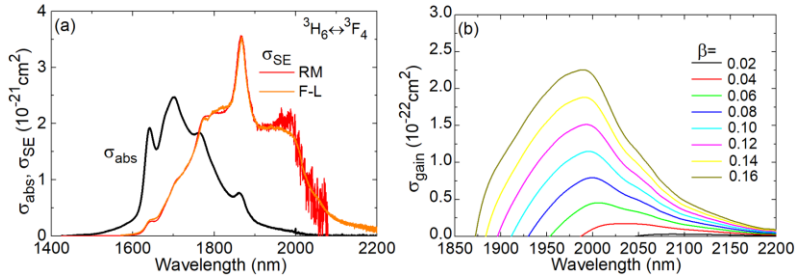

Fig. 9. $^3H_6 \leftrightarrow {}^3F_4$ transition of Tm^{3+} ions in CLTGG: (a) absorption, σ_{abs}, and stimulated emission (SE), σ_{SE}, cross-sections; (b) gain cross-sections, $\sigma_{gain} = \sigma_{SE} - (1 - \beta)\sigma_{abs}$, where $\beta = N_2(^3F_4)/N_{Tm}$ is the inversion ratio.

6. Diode-pumped laser operation

6.1 Laser set-up

Figure 10(a) shows the scheme of the compact diode-pumped Tm:CLTGG laser. The laser element was cut along the [111] direction. It had an aperture of 3.05×3.09 mm^2 and a thickness of 8.19 mm. Both end faces of the element were polished to laser quality and left uncoated. To remove the heat released during pumping, the element was wrapped in indium foil and fixed in a Cu-holder cooled by circulating water; the water temperature was 12 °C.

The laser cavity consisted of a flat pump mirror (PM) coated for high transmission (HT) at 0.80 μm and high reflection (HR) at 1.8-2.1 μm and a set of flat output couplers (OCs) having transmissions T_{OC} of 1.5%, 3%, 5% or 9% at the laser wavelength. Both mirrors were placed

close to the crystal resulting in a geometrical cavity length of ~8.5 mm. The pump source comprised a fiber-coupled (fiber core diameter: 200 μm, N.A. = 0.22) AlGaAs diode laser emitting unpolarized output at a central wavelength of 793 nm (emission bandwidth: 5 nm, M^2 > 80). The pump beam was collimated and focused into the laser element by an AR-coated lens assembly (reimaging ratio: 1:1, f = 30 mm). The pump spot size in the focus $2w_P$ was 200 μm. The measured pump absorption was ~47%. The residual pump was filtered out using a long pass filter (FEL1000, Thorlabs). The spectra of the laser output were measured using a spectrometer (WaveScan, APE). The profile of the laser mode in the far-field was captured using a FIND-R-SCOPE near-IR camera (model 85726).

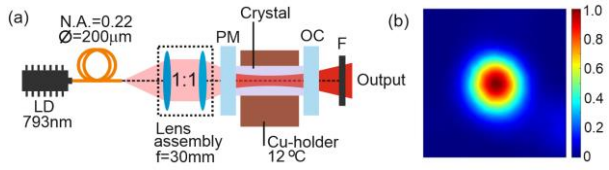

Fig. 10. (a) Scheme of the diode-pumped compact Tm:CLTGG laser: LD – laser diode, PM – pump mirror, OC – output coupler, F – cut-on filter; (b) far-field output profile of the laser mode, T_{OC} = 5%, P_{abs} = 4.0 W.

6.2 Laser performance

The input-output dependences of the diode-pumped Tm:CLTGG laser are shown in Fig. 11(a). The laser generated a maximum output power of 1.08 W at 1995 and 2003 nm with a slope efficiency η of 23.8% (with respect to the absorbed pump power) and a laser threshold of 0.91 W (for T_{OC} = 5%). At the maximum incident pump power of 11.7 W, the optical-to-optical conversion efficiency η_{opt} amounted to 9.2%. Further power scaling was limited by the thermal roll-over in the output dependences. With increasing the output coupling, the laser threshold increased from 0.68 W (T_{OC} = 1.5%) to 1.46 W (T_{OC} = 9%).

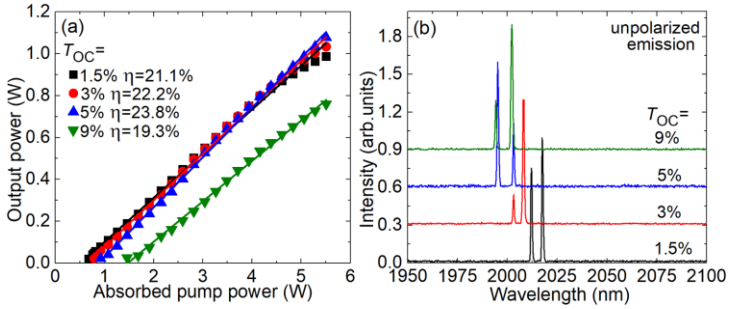

Fig. 11. Diode-pumped Tm:CLTGG laser: (a) input-output dependences, η – slope efficiency; (b) typical spectra of unpolarized laser emission measured at maximum P_{abs}.

Table 5. Laser Performances[a] of Tm^{3+}-doped Gallium Garnets

Crystal	Tm, at.%	P_{out}, W	λ_L, nm	η, %	P_{th}, W	Ref.
Tm:CLTGG	3.17	1.08	1995, 2003	23.8	0.91	This work
Tm:CNNGG	3.2	1.05	2008	35.0	0.39	[8]
Tm:CLNGG	3.6	1.32	2002	45.8	0.30	[8]
	~3	1.6	1985-2015	37	~1	[26]
Tm:CNGG	2.0	0.17	-	3.9	3.5	[27]
	-	0.02	1980-2015	-	4	[28]

[a] P_{out} - output power, λ_L - laser wavelength, η -slope efficiency, P_{th} - laser threshold.

The laser generated unpolarized emission. The typical spectra of the laser emission are shown in Fig. 11(b). With increasing T_{OC} from 1.5% to 9%, a blue shift of the emission

wavelength was observed from 2012 and 2017 nm to 1994 and 2002 nm. This shift is due to the decreasing reabsorption losses in the crystal typical for quasi-three-level Tm lasers. It also agrees with the gain spectra of Tm:CLTGG, cf. Fig. 9(b). The dual-wavelength emission was due to the etalon effect at the crystal / mirror interface and the broad and smooth gain profile.

The laser mode in the far-field, Fig. 10(b), was nearly circular.

A summary of output characteristics of CW lasers based on Tm^{3+}-doped disordered gallium garnets is presented in Table 5.

7. Conclusions

To conclude, Tm:CLTGG is a promising crystal for ultrashort pulse generation (sub-100 fs) in the eye-safe spectral range of ~2 μm. It exhibits a structural disorder related to a random site distribution of Ta^{5+}, Ga^{3+} and Li^{+} cations over the same lattice sites, octahedral (16*a*) and tetrahedral (24*d*), which leads to a significant inhomogeneous broadening of the absorption and emission bands of Tm^{3+} ions confirmed at low temperature (10 K). At room temperature, due to a combination of the inhomogeneous broadening and electron-phonon interaction, Tm:CLTGG exhibits smooth and very broad gain profiles owing to the phonon-assisted $^3F_4 \rightarrow {}^3H_6$ transition extending up to at least ~2.2 μm. From X-ray diffraction, Raman spectroscopy and optical transmission, it is evident that Li^{+} ions provide charge compensation during the heterovalent doping (as Tm^{3+} ions are replacing Ca^{2+} ones) and almost eliminate the presence of cationic vacancies. Finally, Tm:CLTGG exhibits attractive thermal properties (for a disordered crystal) being superior to those of the CNGG-type crystals.

Funding. This work was supported by Spanish Government, Ministry of Science and Innovation (project No. PID2019-108543RB-I00) and by Generalitat de Catalunya (project No. 2017SGR755). National Natural Science Foundation of China (52072351); Foundation of the President of China Academy of Engineering Physics (YZJJLX2018005); Foundation of Key Laboratory of Optoelectronic Materials Chemistry and Physics, Chinese Academy of Sciences (2008DP173016); Foundation of State Key Laboratory of Crystal Materials, Shandong University (KF2001).

Disclosures. The authors declare no conflicts of interest.

Data Availability. Data underlying the results presented in this paper are not publicly available at this time but may be obtained from the authors upon reasonable request.

References

1. J. M. Cano-Torres, M. Rico, X. Han, M. D. Serrano, C. Cascales, C. Zaldo, V. Petrov, U. Griebner, X. Mateos, P. Koopmann, and C. Kränkel, "Comparative study of crystallographic, spectroscopic, and laser properties of Tm^{3+} in $NaT(WO_4)_2$ (T = La, Gd, Y, and Lu) disordered single crystals," Phys. Rev. B **84**(17), 174207-1-15 (2011).
2. A. Lupei, V. Lupei, L. Gheorghe, L. Rogobete, E. Osiac, and A. Petraru, "The nature of nonequivalent Nd^{3+} centers in CNGG and CLNGG," Opt. Mater. **16**(3), 403-411 (2001).
3. W. Jing, P. Loiko, J. M. Serres, Y. Wang, E. Vilejshikova, M. Aguiló, F. Díaz, U. Griebner, H. Huang, V. Petrov, and X. Mateos, "Synthesis, spectroscopy, and efficient laser operation of "mixed" sesquioxide $Tm:(Lu,Sc)_2O_3$ transparent ceramics," Opt. Mater. Express **7**(11), 4192-4202 (2017).
4. Yu. K. Voronko, A. A. Sobol, A. Y. Karasik, N. A. Eskov, P. A. Rabochkina, and S. N. Ushakov, "Calcium niobium gallium and calcium lithium niobium gallium garnets doped with rare earth ions – effective laser media," Opt. Mater. **20**(3), 197–209 (2002).
5. E. Castellano-Hernández, M. D. Serrano, R. J. Jiménez Riobóo, C. Cascales, C. Zaldo, A. Jezowski, and P. A. Loiko, "Na modification of lanthanide doped $Ca_3Nb_{1.5}Ga_{3.5}O_{12}$-type laser garnets: Czochralski crystal growth and characterization," Cryst. Growth Des. **16**(3), 1480–1491 (2016).
6. Yu. K. Voron'ko, A. B. Kudryavtsev, N. A. Es'kov, V. V. Osiko, A. A. Sobol', E. V. Sorokin, and F. M. Spiridonov, "Raman scattering of light in crystals and melt of calcium-niobium gallium garnet," Sov. Phys. Dokl. **32**(1), 70–73 (1988).
7. M. D. Serrano, J. O. Álvarez-Pérez, C. Zaldo, J. Sanz, I. Sobrados, J. A. Alonso, C. Cascales, M. T. Fernández Díaz, and A. Jezowski, "Design of Yb^{3+} optical bandwidths by crystallographic modification of disordered calcium niobium gallium laser garnets," J. Mater. Chem. C **5**(44), 11481–11495 (2017).
8. Z. Pan, J. M. Serres, E. Kifle, P. Loiko, H. Yuan, X. Dai, H. Cai, M. Aguiló, F. Díaz, Y. Wang, Y. Zhao, U. Griebner, V. Petrov, and X. Mateos, "Comparative study of the spectroscopic and laser properties of Tm^{3+}, $Na^{+}(Li^{+})$-codoped $Ca_3Nb_{1.5}Ga_{3.5}O_{12}$-type disordered garnet crystals for mode-locked lasers," Opt. Mater. Express **8**(8), 2287-2299 (2018).

9. J. O. Álvarez-Pérez, J. M. Cano-Torres, A. Ruiz, M. D. Serrano, C. Cascales, and C. Zaldo, "A roadmap for laser optimization of Yb:$Ca_3(NbGa)_5O_{12}$-CNGG-type single crystal garnets," J. Mater. Chem. C **9**(13), 4628-4642 (2021).
10. Z. Pan, Y. Wang, Y. Zhao, H. Yuan, X. Dai, H. Cai, J. E. Bae, S. Y. Choi, F. Rotermund, X. Mateos, J. Maria Serres, P. Loiko, U. Griebner, and V. Petrov, "Generation of 84-fs pulses from a mode-locked Tm:CNNGG disordered garnet crystal laser," Photon. Res. **6**(8), 800-804 (2018).
11. Z. Pan, Y. Wang, Y. Zhao, M. Kowalczyk, J. Sotor, H. Yuan, Y. Zhang, X. Dai, H. Cai, J. E. Bae, S. Y. Choi, F. Rotermund, P. Loiko, J. M. Serres, X. Mateos, U. Griebner, and V. Petrov, "Sub-80 fs mode-locked Tm,Ho-codoped disordered garnet crystal oscillator operating at 2081 nm," Opt. Lett. **43**(20), 5154-5157 (2018).
12. Z. Pan, P. Loiko, Y. Wang, Y. Zhao, H. Yuan, K. Tang, X. Dai, H. Cai, J. M. Serres, S. Slimi, E. B. Salem, E. Dunina, A. Kornienko, L. Fomicheva, J. L. Doualan, P. Camy, W. Chen, U. Griebner, V. Petrov, M. Aguiló, F. Díaz, R. M. Solé, and X. Mateos, "Disordered Tm^{3+}, Ho^{3+}-codoped CNGG garnet crystal: Towards efficient laser materials for ultrashort pulse generation at ~2 μm," J. Alloys Compd. **853**, 157100-1-15.
13. Y. Zhao, Y. Wang, W. Chen, Z. Pan, L. Wang, X. Dai, H. Yuan, Y. Zhang, H. Cai, J. E. Bae, S. Y. Choi, F. Rotermund, P. Loiko, J. M. Serres, X. Mateos, W. Zhou, D. Shen, U. Griebner, and V. Petrov, "67-fs pulse generation from a mode-locked Tm,Ho:CLNGG laser at 2083 nm," Opt. Express **27**(3), 1922-1928 (2019).
14. C. Ma, Y. Wang, X. Cheng, M. Xue, C. Zuo, C. Gao, S. Guo, and J. He, "Spectroscopic, thermal, and laser properties of disordered garnet Nd:CLTGG crystal," J. Cryst. Growth **504**, 44-50 (2018).
15. G. Q. Xie, D. Y. Tang, W. D. Tan, H. Luo, S. Y. Guo, H. H. Yu, and H. J. Zhang, "Diode-pumped passively mode-locked Nd:CTGG disordered crystal laser," Appl. Phys. B **95**(4), 691-695 (2009).
16. F. Lou, S. Y. Guo, J. L. He, B. T. Zhang, J. Hou, Z. W. Wang, X. T. Zhang, K. J. Yang, R. H. Wang, and X. M. Liu, "Diode-pumped passively mode-locked femtosecond Yb:CTGG laser," Appl. Phys. B **115**(2), 247-250 (2014).
17. B. R. Judd, "Optical absorption intensities of rare-earth ions," Phys. Rev. **127**(3), 750–761 (1962).
18. G. S. Ofelt, "Intensities of crystal spectra of rare-earth ions," J. Chem. Phys. **37**(3), 511–520 (1962).
19. P. Loiko, A. Volokitina, X. Mateos, E. Dunina, A. Kornienko, E. Vilejshikova, M. Aguilo, and F. Diaz, "Spectroscopy of Tb^{3+} ions in monoclinic $KLu(WO_4)_2$ crystal: application of an intermediate configuration interaction theory," Opt. Mater. **78**, 495-501 (2018).
20. S. Guo, D. Yuan, X. Zhang, X. Cheng, F. Yu, and X. Tao, "Growth and characterizations of calcium tantalum gallium garnet single crystal," J. Cryst. Growth **311**(1), 214-217 (2008).
21. B. M. Walsh, N. P. Barnes, and B. Di Bartolo, "Branching ratios, cross sections, and radiative lifetimes of rare earth ions in solids: Application to Tm^{3+} and Ho^{3+} ions in $LiYF_4$," J. Appl. Phys. **83**(5), 2772–2787 (1998).
22. P. S. Peijzel, P. Vergeer, A. Meijerink, M. F. Reid, L. A. Boatner, and G. W. Burdick, "$4f^{n-1}5d \rightarrow 4f^n$ emission of Ce^{3+}, Pr^{3+}, Nd^{3+}, Er^{3+}, and Tm^{3+} in $LiYF_4$ and YPO_4," Phys. Rev. B **71**(4), 045116-1-9 (2005).
23. A. Lupei, V. Lupei, S. Grecu, C. Tiseanu, and G. Boulon, "Crystal-field levels of Tm^{3+} in gadolinium gallium garnet," J. Appl. Phys. **75**(9), 4652-4657 (1994).
24. B. Aull and H. Jenssen, "Vibronic interactions in Nd:YAG resulting in nonreciprocity of absorption and stimulated emission cross sections," IEEE J. Quantum Electron. **18**(5), 925–930 (1982).
25. S. A. Payne, L. L. Chase, L. K. Smith, W. L. Kway, and W. F. Krupke, "Infrared cross-section measurements for crystals doped with Er^{3+}, Tm^{3+}, and Ho^{3+}," IEEE J. Quantum Electron. **28**(11), 2619–2630 (1992).
26. W. L. Gao, G. Q. Xie, J. Ma, M. N. Liu, P. Yuan, L. J. Qian, H. H. Yu, H. J. Zhang, and J. Y. Wang, "Efficient 2 μm Tm:CLNGG disordered crystal laser," Opt. Mater. **35**(4), 715-717 (2013).
27. Y. Xue, N. Li, D. Wang, Q. Wang, B. Liu, Q. Song, D. Li, X. Xu, H. Gu, Z. Qin, and G. Xie, "Spectroscopic and laser properties of Tm:CNGG crystals grown by the micro-pulling-down method," J. Lumin. **213**, 36-39 (2019).
28. Y. K. Voronko, S. B. Gessen, N. A. Es' kov, A. G. Okhrimchuk, D. V. Smolin, A. A. Sobol, S. N. Ushakov, L. I. Tsymbal, and A. V. Shestakov, "Continuous lasing at a 2 μm wavelength in calcium niobium gallium garnet crystals at room temperature," Quantum Electron. **26**(3), 222-223 (1996).